Observation of Long Supershear Rupture During the Magnitude 8.1 Kunlunshan Earthquake

Michel Bouchon, *et al.*

Science **301**, 824 (2003);
DOI: 10.1126/science.1086832

Science (print ISSN 0036-8075; online ISSN 1095-9203) is published weekly, except the last week in December, by the American Association for the Advancement of Science, 1200 New York Avenue NW, Washington, DC 20005.

(~3000 m depth), below which abyssal waters are devoid of detectable reflections (Fig. 4). Because this feature is consistent in the sections, we speculate that the transition from reflective to transparent waters at ~3000 m depth may represent the boundary between Labrador Sea Water and Norwegian-Greenland Overflow Water of the Deep Western Boundary Current (*22, 23*).

The ability to create detailed images of thermohaline structure in the ocean with low-frequency marine seismic reflection techniques adds a promising new tool for studies of oceanographic processes. The structures imaged in our North Atlantic transects have important implications for oceanic mixing and exchange processes and raise the possibility that the boundaries of deep water masses such as North Atlantic Bottom Water can be mapped seismically. Low-frequency seismic reflection techniques appear well-tuned to image thermohaline fine structure, provided that layers are at least 5 m thick and laterally continuous over hundreds of meters. Reflection techniques offer several advantages—including enhanced lateral resolution (trace spacing of ~6 m), the ability to simultaneously image large sections of the ocean, and opportunities for three-dimensional and time-lapse imaging—that make them an ideal complement to more traditional methods of probing the ocean, which are more limited in their space-time resolution. Finally, our results imply that the extensive global archive of marine seismic reflection data constitutes a large, untapped resource for probing ocean structure.

References and Notes

1. H. Stommel, K. N. Federov, *Tellus* **19**, 306 (1967).
2. R. D. Pingree, *Deep Sea Res.* **16**, 275 (1969).
3. R. W. Schmitt, H. Perkins, J. D. Boyd, M. C. Stalcup, *Deep Sea Res.* **34**, 1655 (1987).
4. T. M. Joyce, *Deep Sea Res.* **23**, 1175 (1976).
5. T. M. Joyce, *J. Phys. Oceanogr.* **7**, 626 (1977).
6. T. M. Joyce, W. Zenk, J. M. Toole, *J. Geophys. Res.* **83**, 6093 (1978).
7. D. Rudnick, R. Ferrari, *Science* **283**, 526 (1999).
8. J. Gonella, D. Michon, *C. R. Acad. Sci. Paris Ser. II* **306**, 781 (1988).
9. J. D. Phillips, D. F. Dean, in *Ocean Variability and Acoustic Propagation*, J. Potter, A. Warn-Varnas, Eds. (Kluwer Academic, Dordrecht, Netherlands, 1991), pp. 199–214.
10. L. R. Haury, M. G. Briscoe, M. H. Orr, *Nature* **278**, 312 (1979).
11. P. H. Wiebe, T. K. Stanton, M. C. Benfield, D. G. Mountain, C. H. Greene, *IEEE J. Ocean. Eng.* **22**, 445 (1997).
12. The observed reflections are coherent in both the shot and CMP domains, and thus cannot be seafloor multiples from previous shots, which are coherent only in the shot domain.
13. We have not applied migration (a process that places dipping events in their proper spatial position) to the images shown. However, because of the small dips of reflectors, migration does not change the images appreciably. We show unmigrated sections because migration artifacts from the seafloor reflection, which has a much higher amplitude than the water column reflections, degrades the deeper portions of migrated sections.
14. The sound source was a 140-liter, 20-element airgun array, and reflections were recorded on a 480-channel, 6-km-long hydrophone streamer. Data were digitized at a sample interval of 4 ms and have a frequency content of 10 to 100 Hz, with a peak frequency near 40 Hz.
15. R. W. Schmitt, D. T. Georgi, *J. Mar. Res.* **40** (suppl.), 659 (1982).
16. D. T. Georgi, R. W. Schmitt, *J. Phys. Oceanogr.* **13**, 632 (1983).
17. Using data corrected for spherical divergence, we calculated the reflection coefficient of the seafloor as $-A_{mult}/A_{sf}$, where A_{mult} is the amplitude of the first seafloor multiple and A_{sf} is the amplitude of the seafloor reflection (*18*). We then calculated reflection coefficients in the water column from the ratio of the amplitudes of water column reflections and the seafloor reflection.
18. M. Warner, *Tectonophysics* **173**, 15 (1990).
19. C. Garrett, W. Munk, *Annu. Rev. Fluid Mech.* **11**, 339 (1979).
20. Because the profiles are collected by a ship traveling at a rate of about 8 km/hour, the images can only be regarded as instantaneous "snapshots" at local scales of about 2 km.
21. B. Ruddick, K. Richards, *Prog. Oceanogr.* **56**, 499 (2003).
22. R. S. Pickart, W. M. Smethie, J. R. N. Lazier, E. P. Jones, W. J. Jenkins, *J. Geophys. Res.* **101**, 20711 (1996).
23. R. S. Pickart, *Deep Sea Res.* **29**, 1553 (1992).
24. P. Wessel, W. H. F. Smith, *Eos* **72**, 441 (1991).

25. We thank the captain and crew of the R/V *Maurice Ewing* for a successful cruise, and A. Gorman, D. Lizarralde, J. Stennett, K. Polzin, T. Joyce, E. Montgomery, and D. Shillington for helpful conversations. B. Tucholke, K. Louden, J. Hopper, H. C. Larsen, and H. van Avendonk contributed to data acquisition. Data were processed using Sioseis, Paradigm's Focus software, and Generic Mapping Tools (*24*). Supported by NSF grants OCE-9819599 (W.S.H.) and OCE-0081502 (R.W.S.).

31 March 2003; accepted 29 May 2003

Observation of Long Supershear Rupture During the Magnitude 8.1 Kunlunshan Earthquake

Michel Bouchon* and Martin Vallée

The 2001 Kunlunshan earthquake was an extraordinary event that produced a 400-km-long surface rupture. Regional broadband recordings of this event provide an opportunity to accurately observe the speed at which a fault ruptures during an earthquake, which has important implications for seismic risk and for understanding earthquake physics. We determined that rupture propagated on the 400-km-long fault at an average speed of 3.7 to 3.9 km/s, which exceeds the shear velocity of the brittle part of the crust. Rupture started at sub–Rayleigh wave velocity and became supershear, probably approaching 5 km/s, after about 100 km of propagation.

The Kunlunshan earthquake that hit Tibet on 14 November 2001 produced the longest rupture yet observed for an earthquake on land. The mapped surface break of the earthquake extends for ~400 km (*1*, *2*). The exceptional length of this event and the presence of several regional broadband stations of the China Digital Seismic and Incorporated Research Institutions for Seismology (IRIS) networks provide a unique opportunity to determine the speed at which rupture propagates on a fault during an earthquake. In the past, it has been thought that earthquake rupture can only propagate at speeds below the Rayleigh-wave velocity of crustal rocks, which, at about 0.92 times the shear (*S*)–wave velocity, lies in the range of 3.0 to 3.2 km/s for the brittle part of the crust. This belief was backed by fracture dynamics theory, which shows that a rupture cannot propagate at a speed between the Rayleigh-wave and *S*-wave velocities. However, more recent works (*3*–*5*) show that, although the range of velocity between the Rayleigh and *S* waves is not allowed, shear cracks can theoretically propagate at intersonic speeds; that is, at speeds between the *S*-wave and the pressure (*P*)–wave velocities. Subsequent theoretical (*6*–*8*) and experimental (*9*, *10*) studies in fracture dynamics confirm these findings.

Values of rupture velocity inferred from studies of earthquakes support the Rayleigh velocity limit to earthquake rupture with a few exceptions of reported observations of supershear rupture (*11*–*15*). Although these observations have not been fully accepted, they have nevertheless generated strong interest in understanding conditions that can lead to supershear rupture (*16*, *17*) and in assessing its seismic risk consequences (*18*).

The Kunlunshan earthquake was recorded in Tibet and surrounding regions by broadband seismic stations (fig. S1). These stations lie at distances between 600 and 1900 km from the fault, a distance range at which the records are dominated by surface (Rayleigh and Love) waves and, especially, because of the strike-slip mechanism of the

Université Joseph Fourier and Centre National de la Recherche Scientifique, Laboratoire de Géophysique Interne et Tectonophysique, Boîte postale 53, 38041 Grenoble, France.

*To whom correspondence should be addressed. E-mail: Michel.Bouchon@ujf-grenoble.fr

earthquake, by Love waves. We used these surface waves to infer the rupture velocity of the earthquake. To do this, we needed to determine the travel-time velocity of Love waves along the various source-station paths.

A year before the Kunlunshan earthquake, an earthquake of magnitude 5.4 occurred in the epicentral area of the Kunlunshan earthquake. We used records from this 5.4 earthquake (fig. S1) to determine the one-dimensional lithospheric velocity structure beneath the fault and receivers. We divided the lithosphere into 5-km-thick layers and inverted the *S*-wave velocity in each layer. This inversion was carried out independently for each station and was based on matching the observed records of the earthquake with the ones calculated by the discrete wave number method (*19*). Because Love waves are polarized transverse to their direction of propagation, we used the record component at each station that is transverse to the epicenter-station path. As the main shock records contain mostly energy at periods longer than 20 s, we low-pass filtered the records above 20 s. We obtained good fits to the waveforms and *S*-wave velocity models (fig. S1 and table S1) that represent the crustal or lithospheric structure averaged over the paths from the source to each station. The crustal thickness of the models ranges from 50 km for paths to northeastern China (the BJT station) and Mongolia (the ULN station) to 65 km for paths almost entirely across the Tibetan Plateau (the LSA and KMI stations).

Knowing the velocity structure, we then simulated the earthquake rupture and calculated the resulting ground motion at each station. We modeled the Kunlunshan earthquake as a rupture that started at the hypocenter and propagated radially on the fault. The N99°E fault plane is vertical and follows the mapped surface breaks (*1*, *2*). The fault slip (fig. S2) is the one measured in the field (*2*) and is assumed to be uniform with depth. To the east, the fault model extends to the end of the mapped surface rupture (94°47.706′E, 35°33.387′N) (*2*). To the west, it ends 15 km west of the U.S. Geological Survey epicentral location (90°32.4′E, 35°57.0′N), giving the fault rupture a total length of 400 km. The precise western termination of the fault, which is not well recognized in the field, is not critical, because slip west of the epicenter is small and did not radiate much seismic energy. The hypocentral depth was set at 15 km, but the synthetic records are unsensitive to it. The calculated waveforms are also unsensitive to the bottom depth of the fault. For the ground-motion calculation, which we performed with the discrete wave number method (*19*), the fault plane was discretized into point sources located at 2-km intervals along the strike and along the depth. At each point, slip began at the arrival of the rupture front and was assumed to grow at a constant rate for 5 s, after which time it reached the value measured in the field. This choice of rise time corresponds to an average slip velocity of about 1 m/s over the fault and is based on previous studies of large earthquakes (*15*, *20*).

We first determined how well a near-Rayleigh rupture velocity could explain the observed Love-wave records. This comparison between synthetics and data is shown (Fig. 1A) for the stations that lay in the forward direction relative to the propagating rupture and that, for this reason, were highly sensitive to the rupture velocity. The velocity considered was 3 km/s, which is close to the Rayleigh velocity of the upper crust. For this value, the timing of the synthetics did not match the timing of the observed waveforms. When we lowered the rupture velocity below 3 km/s, the fit to the data deteriorated further.

To infer the rupture velocity, we divided the 400-km-long fault into four 100-km-long segments and performed a grid search to determine the values that best fit the observations. The best fit obtained (Fig. 1B) corresponds to an average rupture velocity of 3.9 km/s, with a sub-Rayleigh velocity of 2.4 km/s on the first segment and supershear velocities close to 5 km/s on the other three segments. An independent inversion of each record separately yielded results consistent with a rupture that is sub-Rayleigh on the first segment and supershear on the other three. Calculations done with a single 400-km-long segment (i.e., not allowing for spatial variations in rupture velocity) yielded a rupture velocity of 3.7 to 3.8 km/s, regardless of the stations considered.

One of the recording stations, WMQ, lies in the back azimuth relative to the propagating rupture. As a result, the various arrivals there were more spread out in time (Fig. 2A) and two of them can be identified: The first pulse of the Love-wave train originated from the epicentral area, whereas the largest pulse of the wave train was radiated from the fault area that slipped the most during the earthquake. The time difference between these two phases provides a constraint on the rupture velocity. To determine it, we again divided the fault into four 100-km-long segments and performed a grid search that allowed the rupture to vary between 2 and 6 km/s on each segment. The best fit to the record (Fig. 2A) is obtained for a sub-Rayleigh velocity of 2.8 km/s on the first segment and a supershear velocity of 5 km/s on the second and third segments. Rupture velocity on the last segment is poorly resolved, because the records at WMQ are not sensitive to rupture on this part of the fault, where slip is smaller and which lies further from the station. Rupture velocity values on the first three segments yielded an average rupture speed of 3.9 km/s for the first 300 km of rupture. A grid search performed for a single 400-km-long segment with uniform rupture velocity yielded the same value.

The remaining station, LSA, is the one closest to the source and is located in a direction almost perpendicular to the fault. This location provides a wide-angle view of the fault. The horizontal motion displayed at the station in different time windows (Fig. 2, B to E) shows how the direction of incoming seismic energy changes with time. The first window corresponds to the first seconds of energy arrival from the earthquake. This energy travels as *P* waves, which are polarized in the direction of

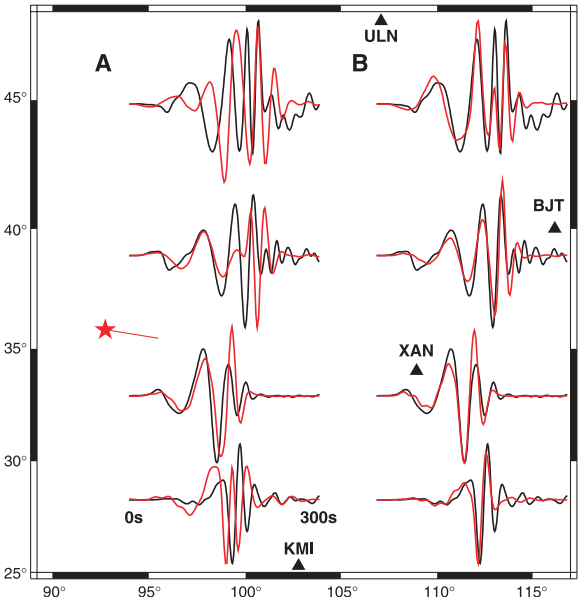

Fig. 1. Comparison between the recorded ground motion (in black) for the Kunlunshan earthquake and the one calculated (in red) for (**A**) a rupture velocity of 3 km/s and (**B**) the best-fitting rupture velocity, which averages 3.9 km/s. The component shown is the horizontal displacement in the direction transverse to the epicenter-station path; it starts with a reduced time equal to the epicentral distance divided by 4.5 km/s. The epicenter (star), the fault geometry (red line), and the station locations (triangles) are displayed.

propagation so that the horizontal motion displays their incoming direction, which corresponds to the epicentral location (Fig. 2B). The second time window (Fig. 2C) includes the beginning of the Love-wave arrivals, which, being polarized transverse to their travel direction, also point to the epicentral location. The third time window (Fig. 2D) corresponds to the first Love-wave cycle. The horizontal motion is an elongated distorted ellipse, described clockwise as a function of time. This elliptical motion results from a combination of large displacements (Love waves) transverse and small displacements (Rayleigh waves) radial to the travel direction. The axis of the first half of the ellipse runs nearly east-west, whereas the axis of the second half is tilted to the south. This indicates that the direction of the incoming waves rotated clockwise, which in turn shows the eastward propagation along the fault of the source of energy released during the first ~30 s of rupture. The fourth time window (Fig. 2E) displays the horizontal motion between 63 s and 79 s after the beginning of the Love-wave arrivals. The motion is still approximately elliptical, but the ellipse axis has now rotated to a direction that indicates that the corresponding source of energy radiation was approaching the eastern end of the fault. Although a precise estimate of rupture velocity is not possible from the diagrams because of the presence of Rayleigh waves and the long duration of a Love-wave cycle, they indicate that between 60 s and 80 s after the start of rupture, the source of energy was well past the middle of the fault and approaching the easternmost part of the rupture. This requires a fast propagation of the rupture and supports the observations at the other stations.

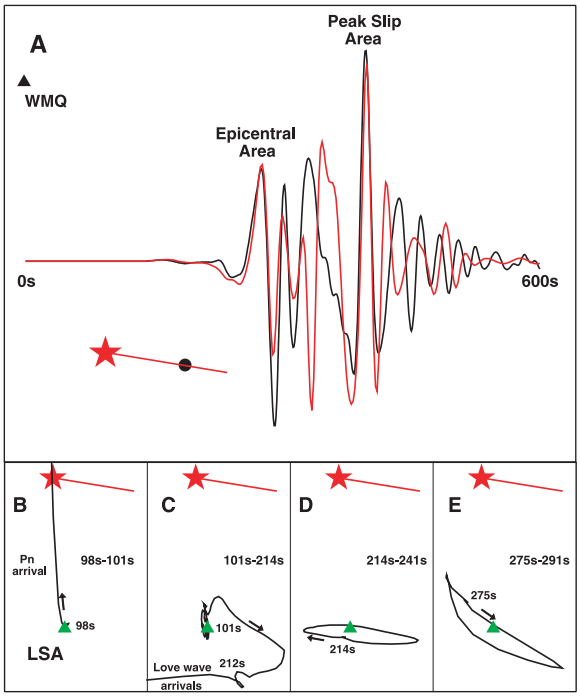

Fig. 2. (**A**) Comparison between the ground motion recorded at WMQ in the direction transverse to the epicenter-station path (in black) with the one calculated (in red) for the best-fitting rupture velocity. The epicenter (star), fault geometry (red line), area of peak slip (black circle), and station location (triangle) are displayed. (**B** to **E**). Time evolution of the horizontal displacement recorded at LSA. The time starts at the origin time of the earthquake. The arrow indicates the evolution of particle motion with increasing time. The polarity of motion in frame (B) is reversed to show the direction of incoming waves. Pn is the first wave arrival.

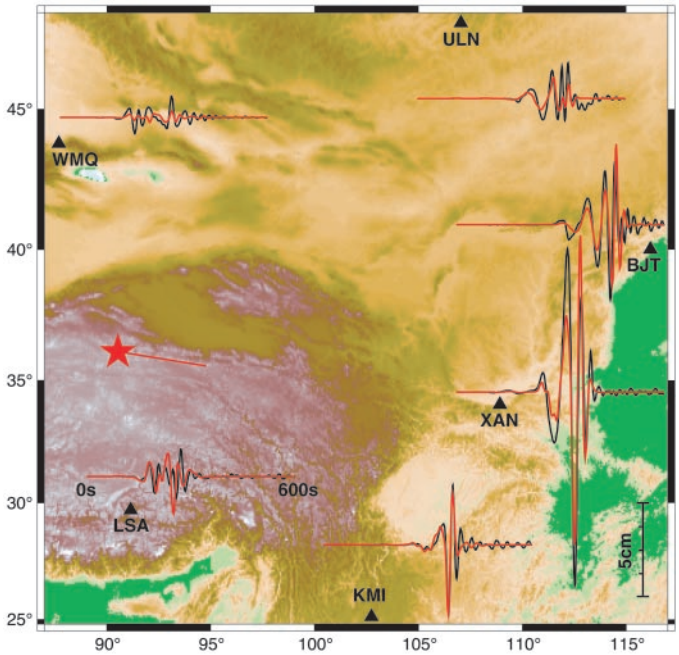

Fig. 3. Comparison of the recorded (black) and computed (red) ground motion in the direction transverse to the epicenter-station paths. A station amplitude correction determined from the amplitude matching of the precursory shock relative to the IRIS station ULN has been applied to the data. Each signal begins 50 s before the *P*-wave arrival and is 600 s long. The depth of faulting is 17 km and the average rupture velocity of the model is 3.9 km/s, with specific values of 2.4, 5.0, 4.8, and 5.0 km/s on the four 100-km-long segments; these individual values are not resolved precisely, but they indicate that rupture started at sub-Rayleigh velocity and became supershear, probably approaching 5 km/s, after some 100 km of propagation.

The elastic energy radiated by the earthquake is closely linked to the rupture velocity. The recorded ground motion displays a strong directivity effect (Fig. 3), because most of the radiated energy is focused along azimuths close to the direction of rupture propagation. This observed azimuthal pattern is explained by the rupture velocity values that we have previously inferred. The amplitude matching between data and synthetics indicates that the seismogenic depth is close to 17 km, which yields a seismic moment of about 6.2×10^{20} N·m.

References and Notes

1. A. Lin *et al.*, *Science* **296**, 2015 (2002).
2. X. Xu, W. Chen, W. Ma, G. Yu, G. Chen, *Seism. Res. Lett.* **73**, 884 (2002).
3. R. Burridge, *Geophys. J.* **35**, 439 (1973).
4. D. J. Andrews, *J. Geophys. Res.* **81**, 5679 (1976).
5. S. Das, K. Aki, *Geophys. J. Roy. Astr. Soc.* **50**, 643 (1977).
6. L. B. Freund, *J. Geophys. Res.* **84**, 2199 (1979).
7. S. M. Day, *Bull. Seism. Soc. Am.* **72**, 1881 (1982).
8. P. G. Okubo, *J. Geophys. Res.* **94**, 12321 (1989).
9. A. J. Rosakis, O. Samudrala, D. Coker, *Science* **284**, 1337 (1999).
10. A. J. Rosakis, O. Samudrala, D. Coker, *Mat. Res. Innovat.* **3**, 236 (2000).
11. R. J. Archuleta, *J. Geophys. Res.* **89**, 4559 (1984).
12. P. Spudich, E. Cranswick, *Bull. Seism. Soc. Am.* **74**, 2083 (1984).
13. K. B. Olsen, R. Madariaga, R. J. Archuleta, *Science* **278**, 834 (1997).
14. W. L. Ellsworth, M. Çelebi, *Am. Geophys. Union, Fall Meeting Suppl.* **80**, F648 (1999).
15. M. Bouchon *et al.*, *Geophys. Res. Lett.* **27**, 3013 (2000).
16. J. Weertman, *Geophys. Res. Lett.* **29**, 109 (2002).
17. E. M. Dunham, P. Favreau, J. M. Carlson, *Science* **299**, 1557 (2003).
18. P. Bernard, *Europ. Seism. Comm. XXVIII Meeting* (2002).
19. M. Bouchon, *Bull. Seism. Soc. Am.* **71**, 959 (1981).
20. R. Madariaga, K. B. Olsen, in *International Handbook of Earthquakes and Engineering Seismology*, W. Lee, H. Kanamori, P. Jennings, C. Kisslinger, Eds. (Academic Press, London, 2002), p. 175.

21. We thank the three anonymous referees for their constructive reviews.

Supporting Online Material
www.sciencemag.org/cgi/content/full/301/5634/824/DC1
Figs. S1 and S2
Table S1

14 May 2003; accepted 3 July 2003